SLAC-PUB-14875

Mode-locked multichromatic x-rays in a seeded free-electron laser for single-shot x-ray spectroscopy

Dao Xiang, Yuantao Ding, Tor Raubenheimer and Juhao Wu
SLAC National Accelerator Laboratory, Menlo Park, CA, 94025, USA
(Dated: May 3, 2012)

We present the promise of generating gigawatt mode-locked multichromatic x-rays in a seeded free electron laser (FEL). We show that by using a laser to imprint periodic modulation in electron beam phase space, a single-frequency coherent seed can be amplified and further translated to a mode-locked multichromatic output in an FEL. With this configuration the FEL output consists of a train of mode-locked ultrashort pulses which span a wide frequency gap with a series of equally spaced sharp lines. This gigawatt multichromatic x-rays may potentially allow one to explore the structure and dynamics of a large number of atomic states simultaneously. The feasibility of generating mode-locked x-rays ranging from Carbon K-edge ($\sim$284 eV) to Copper L_3 edge ($\sim$931 eV) is confirmed with numerical simulation using the realistic parameters of the linac coherent light source (LCLS) and LCLS-II. We anticipate that the mode-locked multichromatic x-rays in FELs may open up new opportunities in x-ray spectroscopy (i.e. resonant inelastic x-ray scattering, time-resolved scattering and spectroscopy, etc.).

PACS numbers: 41.60.Cr

I. INTRODUCTION

Free electron lasers (FELs) can provide high-power coherent short-wavelength radiation which is enabling forefront science in physics, chemistry, biology, material science, etc. In the x-ray wavelengths, most of the FELs operate in the self-amplified spontaneous emission (SASE) mode [1, 2] in which the initial beam shot noise is amplified by several orders of magnitude to gigawatt (GW) and beyond. A SASE FEL is characterized by poor temporal coherence (i.e. noisy in both the temporal profile and the frequency spectrum). There are many applications (in particular the spectroscopic study of correlated electron materials) that require, or could benefit from, improved temporal coherence (i.e. a well-controlled pulse shape and a bandwidth close to the Fourier transform limit).

Introducing a coherent seed to dominate over the shot noise can lead to greatly improved temporal coherence for the FEL output. Currently, both self-seeding [3–6] and external seeding [7–14] are under active study for generation of fully coherent x-rays. Nonetheless, such seeded FELs nominally only provide one frequency line, i.e. a fully coherent output at a specific frequency determined by the monochromator, or the seed laser frequency and the harmonic number. Extension to generation of multiple frequency lines may enhance the capability of FELs in some specific applications (i.e. resonant inelastic x-ray scattering (RIXS [15]) that require scanning the x-ray energy over a small range.

RIXS is a widely used photon-in and photon-out spectroscopic technique for investigation of the properties of correlated electron materials [16–20]. In RIXS, typically the energy of the incoming photons is scanned near one of the atomic x-ray absorption edges, and the properties of the outgoing photons (energy, momentum, and polarization) are measured. RIXS generally requires multi-shot measurements, not only because the technique is photon hungry, but also because it typically requires one to change the energy of the incoming photons used to create excited states. With the advent of x-ray FELs, the photon flux can be increased by orders of magnitude, compared to that from the synchrotrons. Therefore, it may be envisioned that if the output of an FEL can be tailored to provide x-rays which span a wide frequency range covering the absorption edges with multiple sharp lines as those from mode locked lasers, RIXS may be performed in a single-shot with a spectrometer that disperses the incoming and outgoing photons in two orthogonal planes [21]. This may greatly enhance the capability of an x-ray FEL, and may potentially open up new opportunities in x-ray science.

Mode-locked radiation pulses are characterized by the multiple frequency lines with a constant mode spacing (the corresponding distribution in time domain is a periodic short pulse train). The concept of mode locking x-rays in an FEL was first introduced in [22] and further developed in [23, 24]. In these schemes, frequent temporal shift of the radiation field with respect to the electron beam using a series of undulator-chicane sections allows generation of axial modes in an FEL, and modulating the beam energy at the mode spacing frequency with a laser allows all the modes to be locked in phase. However, the temporal shift requires a series of chicanes with moderate strength between undulator sections, which are not readily available in existing x-ray FELs, such as the Linac Coherent Light Source (LCLS) [25] in US, FLASH[26] in Germany and SACLA in Japan [27]. For LCLS-II [28], while there are mini-chicanes available between each undulator section to serve as the phase shifter, the strength is much lower than what required to shift the radiation by many wavelengths, as required in the schemes for mode locking of a SASE FEL.

In this paper we study an alternative scheme to generate mode-locked multichromatic x-rays in a seeded FEL

Work supported in part by US Department of Energy contract DE-AC02-76SF00515.

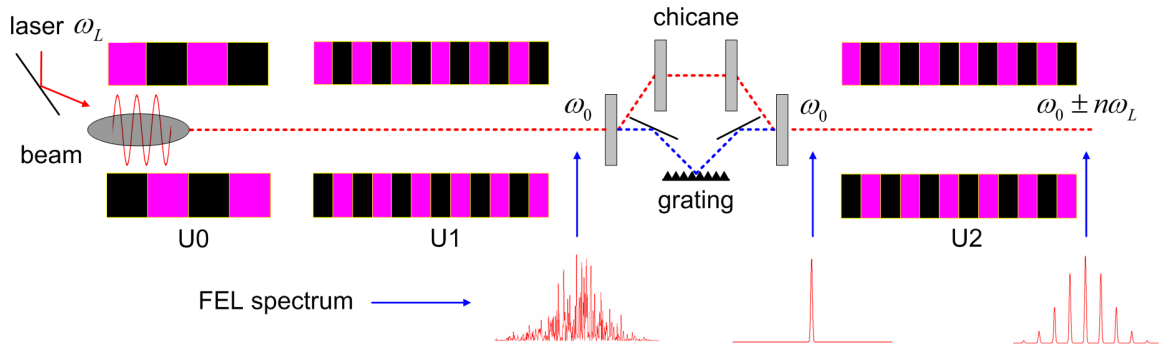

FIG. 1: Schematic for generation of mode-locked multichromatic x-rays in a seeded FEL.

for spectroscopy applications such as single-shot RIXS. It is found that by using a laser to imprint periodic modulation in electron beam phase space, a single-frequency coherent seed can be amplified and further translated to a mode-locked multichromatic output in an FEL. The scheme studied in this paper makes full use of the self-seeding beam line, and greatly simplifies the implementation of a mode locking FEL since it does not require chicanes to frequently shift the radiation. The feasibility of generating mode-locked multichromatic x-rays ranging from Carbon K-edge (∼284 eV) to Copper L-3 edge (∼931 eV) is demonstrated with numerical simulation using the realistic parameters of the LCLS and LCLS-II.

II. METHODS

The method pursued in this paper for generation of mode-locked multichromatic soft x-rays in a seeded FEL is schematically shown in Fig. 1. It consists of 3 undulators (U1, U2 and U3), a grating-based monochromator and a chicane. Except U1, the beam line from U2 to U3 is just the widely adopted configuration for self-seeding [3] in the soft x-ray wavelengths where the output from the SASE FEL in U1 is monochromated and further amplified to saturation in the second undulator U2.

For generation of mode-locked multichromatic x-rays, we propose to add a short undulator U0 upstream of U1 such that a laser with a much longer wavelength $\lambda_L = 2\pi c/\omega_L$ can be used to modulate the energy distribution of the beam, where c is the speed of light and ω_L is the angular frequency of the laser. The energy modulation amplitude is chosen in such a way that it is larger than the beam slice energy spread (for generation of significant density modulation after passing through the chicane), but smaller than the FEL parameter ρ (for minimizing the degradation to FEL gain in U1 from increased energy spread and local energy chirp). At the exit of U1, a grating-based monochromator is used to select a narrow-band radiation (with central angular frequency at ω_0) from the SASE radiation which has a relatively broad spectrum. The chicane introduces additional path length for the electron beam to compensate for the delay (on the order of ∼ ps) of the x-rays in the monochromator. The momentum compaction of the chicane R_{56} also effectively washes out the noisy microbunching developed in U1. Furthermore, it will convert the beam energy modulation imprinted in U0 into density modulation. Finally, the single-frequency coherent seed at ω_0 is amplified by the density-modulated beam in U2 and translated to a mode-locked output with discrete frequencies $\omega_0 \pm n\omega_L$ at the exit of U2, where n is an integer.

The physics behind this scheme is analogous to the active mode locking for an optical laser where a sinusoidal amplitude modulation at the mode spacing frequency of the resonant cavity is used to produce phase-locking of all the modes. Here by modulating the lasing medium (the relativistic electron beam), the amplitude of the coherent seed with carrier frequency at ω_0 is also modulated at the laser frequency ω_L. This leads to the development of sidebands at frequencies $\omega_0 + \omega_L$ and $\omega_0 - \omega_L$, as is well-known in telecommunications. As the amplification continues, the amplitudes of the modes at these sidebands frequencies will also be modulated by the electron beam, which further leads to development of new modes at $\omega_0 + 2\omega_L$ and $\omega_0 - 2\omega_L$. This process repeats and finally the single-frequency coherent seed is translated to a mode-locked output at the exit of U2 with sharp lines at frequencies $\omega_0 \pm n\omega_L$.

Note, the bandwidth of each frequency line depends on the resolving power of the grating and the bunch length. In order to avoid overlapping of the frequency lines (i.e. frequency spacing larger than 3 times the FWHM bandwidth of each frequency line), the electron bunch needs to be at least 6 times longer than the modulation laser wavelength. It is also desirable to have a grating with resolving power matching that of the bunch length such that a single mode is selected after the monochromator. In the time domain, the FEL power profile copies that of the electron current distribution. These ultrashort pulse trains is a natural result of mode locking in which summation of multiple oscillation modes with equal mode spacing leads to a periodic short pulse train with spacing equal to the inverse of the mode spacing.

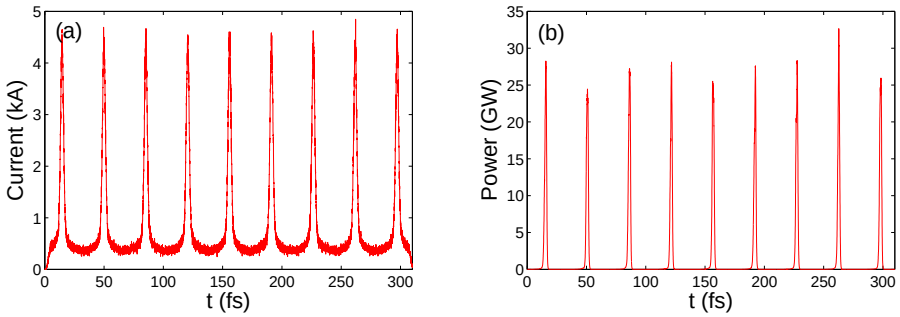

FIG. 2: (a) Beam current distribution at the entrance to U2 (bunch head to the right) and the FEL power profile at the exit of U2 (b).

III. IDEAL CASE

In this section we present the promise of generating mode locking x-rays using a set of ideal parameters. Specifically, we use a beam with no variations in current, energy, energy spread and emittance along the longitudinal direction. The undulator configurations is chosen to be the same as that in LCLS, i.e. there are breaks between each undulator section and the number of undulator period is 110 for each section. The beam and undulator parameters are listed in Table. 1. For simplicity, we do not simulate the beam dynamics upstream of U2. Instead, we generate an ideal density-modulated beam by assuming an 4.2 MeV energy modulation with a 10.6 μm CO_2 laser. We also neglect the undulator wake fields in U2. Fully self-consistent simulations with realistic beams will be presented in Sec. IV.

TABLE I: Parameters of the electron beam and undulators.

Parameter	Symbol	Value	Unit
Beam energy	E	4.583	GeV
Beam charge	Q	250	pC
Normalized transverse emittance	$\epsilon_{nx,ny}$	0.6	μm
Slice energy spread	σ_E	0.7	MeV
Peak current	I_p	800	A
Laser wavelength	λ_L	10.6	μm
Peak energy modulation	Δ_E	4.2	MeV
Chicane momentum compaction	R_{56}	2.65	mm
Undulator period	λ_u	3.3	cm
Undulator K value	K	3.50	

Here we focus on the soft x-rays with photon energy around the Cu L_3 edge (∼931 eV) [19, 20], where fruitful science (of particular interest is the study of high temperature superconductors) lies. We assume that the seed has a power of 50 kW with a central wavelength at $\lambda_0 = 1.333$ nm. The beam current distribution at the entrance to U2 is shown in Fig. 2a. The beam distribution is obtained by sending the beam with 4.2 MeV energy modulation through a chicane with $R_{56} = 2.65$ mm. By converting the energy modulation into density modulation, the beam that initially has constant current now consists of many bumps equally separated by the laser wavelength. Within the current bumps (4.8 kA peak current with 4.2 MeV slice energy spread), the FEL power gain length is about 1.2 m as estimated from Xie's formula [29]. In the current dips, the current is reduced to about 400 A (the slice energy spread is reduced to about 350 keV) and the gain length is about 2.3 m. Accordingly, the FEL power grows much faster in the current bumps than in the dips. As a result, the FEL output after six undulator sections copies that of the current distribution and consists of a train of short x-ray pulses (Fig. 2b).

Because the FEL is seeded with a coherent signal, the output x-ray pulse train is naturally phase-locked and its spectrum will have many discrete lines, as shown in Fig. 3a. The overall spectral bandwidth is related to the temporal duration of each pulse, and the bandwidth of each frequency line is determined by the overall duration of the pulse train (similar to the bunch length). The spacing of the frequency lines $\Delta\omega$ equals to ω_L, the frequency of the CO_2 laser. Fig. 3b provides a detailed view of the central line at 1.333 nm of which the relative FWHM bandwidth is about 1.24×10^{-5} which is approximately the transform limit of a rectangular pulse with 300 fs duration. Fig. 3c is the spectral intensity of the x-ray pulse as a function of photon energy. From Fig. 3c one can see that about 20 sharp lines with a spacing of 117 meV (the photon energy of the CO_2 laser) and FWHM bandwidth of about 12 meV are generated. The number of photons for each spectral line is on the order of $10^{11} \sim 10^{12}$, about 7∼8 orders of magnitude higher than that obtained from a single pulse in a state-of-the-art synchrotron, yet still 2∼3 orders of magnitude lower than what required to obtain a decent spectrum in RIXS. More photons can be generated by increasing the brightness of the electron beam (i.e. higher peak current and lower emittance) or employing a long tapered undulator. This mode-locked multichromatic x-rays together with improvements in increasing x-ray grating efficiency, spectrometer acceptance and detection efficiency may potentially enable single-shot RIXS in the not-too-distant future.

It is worth mentioning that the number of frequency lines approximately equals to the ratio of the FEL band-

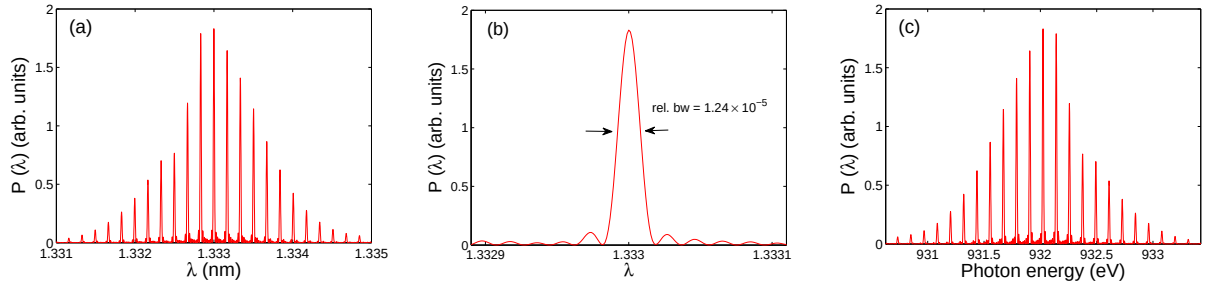

FIG. 3: FEL power spectrum as a function of x-ray wavelength (a); enlarged view of the central frequency line (b); FEL power spectrum as a function of x-ray photon energy (c).

width to the frequency spacing. Accordingly, more spectral lines can be generated with a higher energy modulation. Furthermore, the spacing of the spectral lines can be varied by changing the wavelength of the modulation laser. Therefore, in principle the FEL output can be tailored to meet the demands of a specific application.

It should be pointed out that the above example is just representative. Generation of fully coherent FEL output with 1.24×10^{-5} bandwidth requires a grating with a resolving power of about 80000. This is about 3 times higher than what achieved with current state-of-the-art technology [30]. Simulation of mode-locked x-rays with realistic beam and grating parameters will be presented in Sec. IV.

IV. REALISTIC CASES AT LCLS AND LCLS-II

In this section, we study the feasibility of generating mode-locked multichromatic x-rays at LCLS and LCLS-II using the realistic beam distributions obtained in start-to-end simulations. The quantum diffusion effect in the undulators, the resistive wall wake fields from the undulator pipe, as well as the coherent synchrotron radiation (CSR) effect when the beam passes through the chicane are all included.

As representative examples, we will focus on two radiation wavelengths, one around 4.37 nm (∼284 eV, Carbon K-edge) using the LCLS-II parameters and the other around 1.33 nm (∼931 eV, Copper L_3-edge) using LCLS parameters. Generation of mode-locked x-rays at other soft x-rays wavelengths (i.e. Oxigen K-edge at $\sim$ 530 eV, Iron L-edge at $\sim$ 720 eV, Nickel L-edge at $\sim$ 870 eV, etc.) can be studied similarly.

A. Mode-locked multichromatic x-rays for Carbon K-edge

With variable-gap undulator, the LCLS-II will cover a broader wavelengths of x-rays (>250 eV) than the LCLS (>600 eV), allowing one to reach the Carbon K-edge. In the baseline design of LCLS-II [28], the soft x-ray undulators have 18 sections with a break of 1 m between each undulators. The number of undulators per section is 61 and the undulator period is 5.5 cm. The electron beam distribution used in our study for generating mode-locked multichromatic x-rays is similar to that used in [31] for study of echo-seeding option for LCLS-II, except that here the beam energy is taken to be 4.583 GeV. The beam peak current is about 800 A and the slice energy spread is about 700 keV.

In our study, a 2.6 μm laser with peak power of about 1 GW and rms duration of 60 fs is used to generate 2.1 MeV energy modulation in beam phase space in a short undulator with 6 periods and a period length of 45 cm. Such a laser is readily available from an optical parametric amplifier pumped with Ti:Sapphire laser. The laser energy modulation amplitude is chosen to match the momentum compaction (R_{56}=0.96 mm) of the chicane such that the energy modulation will be effectively converted into density modulation after passing through the chicane. The electron-laser interaction is simulated with the code ELEGANT [32]. After the laser modulation, the particle files are dumped and further used in FEL simulation with GENESIS [33].

We assume the 9th undulator section is replaced with a 4-dipole chicane and a monochromator. The length of the magnet is assumed to be 0.4 m and the distance between the first and second dipole is 0.5 m (and hence that between the third and forth dipole). Such a compact chicane can fit in a 3 m space. If we limit the bending strength of the dipole to 1 T, the maximal R_{56} of the chicane for a ∼4.6 GeV beam is found to be about 1 mm. A typical design of a grating-based monochromator with a delay time matching that of the chicane (note the delay time is $R_{56}/2c$) may provide a resolving power of 7500 [34]. Note, further increasing the resolving power while limiting the delay time to $\sim$ 1.5 ps is possible [35]. Therefore, the results presented in this section should be considered as conservative.

After 8 undulator sections, the FEL power and spectrum are shown in Fig. 4. The quantum diffusion in the undulators and the resistive wall wake field from the undulator chamber [36] are included. The monochromator with 7500 resolving power will select a single spike and the corresponding radiation spectrum and power profile after the monochromator are shown in Fig. 5. Here the

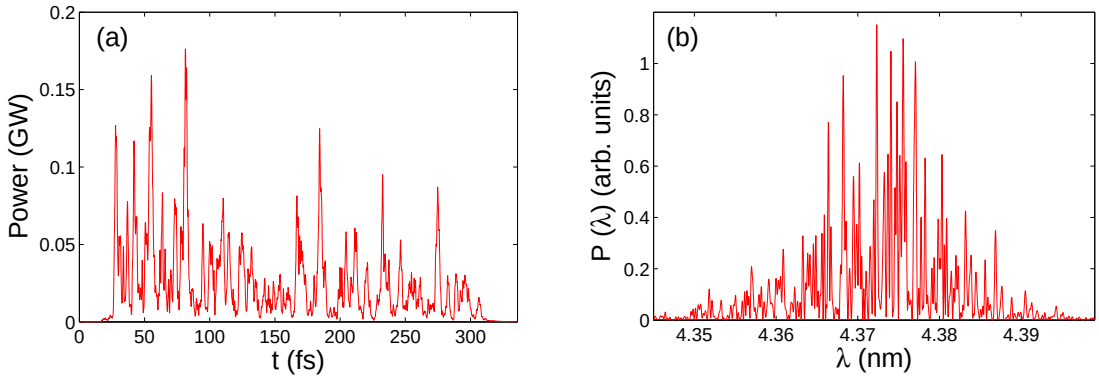

FIG. 4: FEL power (a) and spectrum (b) before the monochromator.

overall efficiency of the monochromator is assumed to be 3%, including the reflectivity of the mirrors and the grating efficiency. The coherent seed after the monochromator is close to a transform limited pulse and will be further amplified in the downstream undulators.

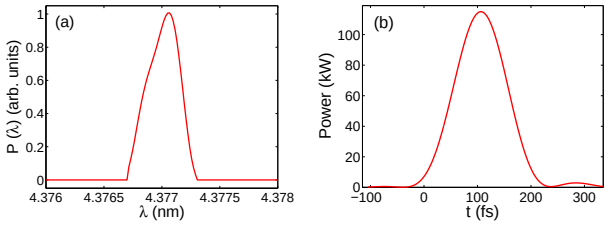

FIG. 5: FEL spectrum (a) and power (b) after the monochromator.

Two unwanted effects may potentially degrade the performance of the proposed scheme. One is energy spread growth from the quantum diffusion and FEL interaction in the undulators before the chicane, the other is the CSR effect in the chicane.

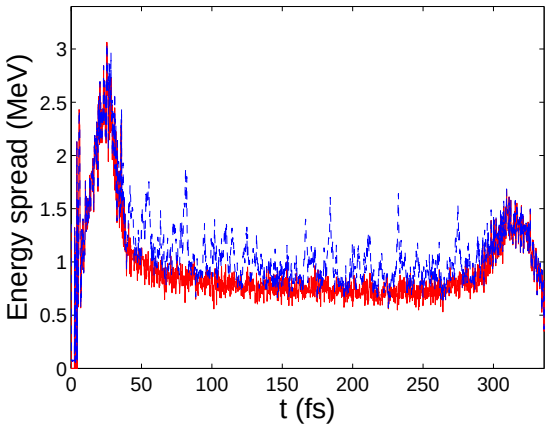

FIG. 6: Electron beam slice energy spread before (red solid line) and after (blue dashed line) the 8 undulator sections.

Note, the proposed scheme relies on generation of significant density modulation in electron beam, which requires the energy modulation to be much larger than beam slice energy spread at the entrance to the chicane. Therefore, the number of undulator sections before the monochromator should be properly chosen to avoid a significant increase in beam slice energy spread from the FEL interaction. In our example, the beam slice energy spread before and after 8 undulator sections is shown in Fig. 6 where one can see that the slice energy spread after FEL interaction is still smaller than the energy modulation. A comparison between Fig. 4a and Fig. 6 indicates that the beam slice energy spread copies the distribution of FEL power. Therefore, measurement of the time-dependent energy distribution of an electron beam after the undulator sections may allow one to obtain the temporal profile of the x-rays [37].

To estimate the potential collective effects when the beam passes through the chicane, the particles are dumped at the exit of the 8th undulator and further

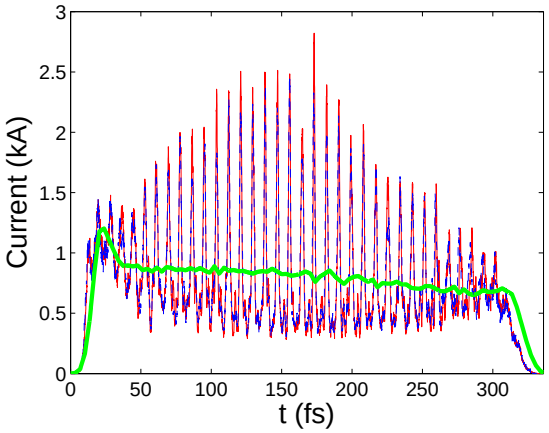

FIG. 7: Electron beam current before (green line) and after the chicane with (blue dashed line) and without (red solid line) the quantum diffusion and FEL interaction in the 8 undulators taken into account.

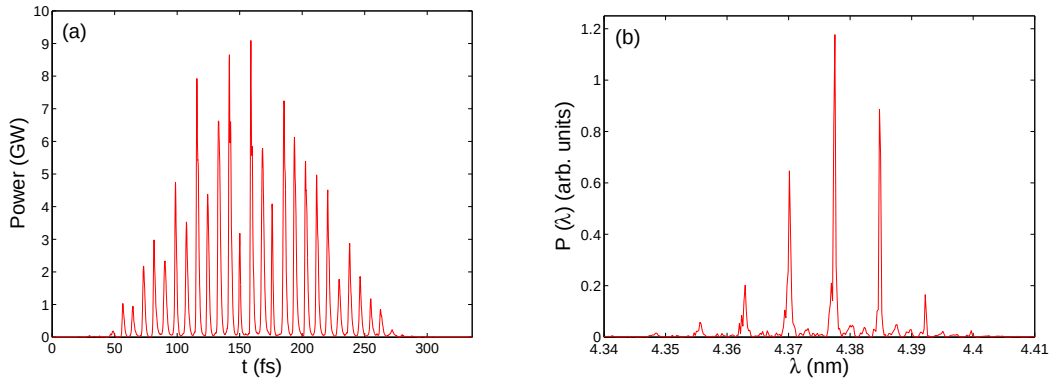

FIG. 8: FEL power and spectrum after the coherent seed is amplified by the density-modulated beam in 7 undulator sections.

imported to ELEGANT code to include the CSR effect. Due to the relatively small momentum compaction of the chicane, other than an average energy loss of about 300 keV, no noticeable effect from CSR on beam slice emittance and slice energy spread was seen in simulation. The beam current distribution after passing through the chicane is shown in Fig. 7 where one can clearly see that the energy modulation is effectively converted into density modulation. A comparison between the blue and red line in Fig. 7 implies that the energy spread growth from the FEL interaction in the upstream undulators slightly reduced the peak current after the chicane. This density modulated beam will be further used to amplify the coherent seed in the downstream undulators.

After passing through the chicane, the particles are again dumped and further imported to GENESIS simulation. After 7 undulator sections, the final output of the mode-locked FEL is shown in Fig. 8. In the time domain, the FEL power profile consists of a train of short pulses with FWHM duration of about 1.2 fs and a spacing of 8.67 fs (corresponding to the wavelength of the modulation laser). In the frequency domain, the FEL spectrum consists of equally spaced sharp lines with FWHM bandwidth of about 1×10^{-5} and a mode spacing of 0.43 eV.

It should be pointed out that the mode-locked output is only possible when the FEL starts with a coherent seed. Without a coherent seed, it is just the current-enhanced SASE case [38]. For convenience of comparison, the SASE FEL power and spectrum with this density modulated beam are shown in Fig. 9.

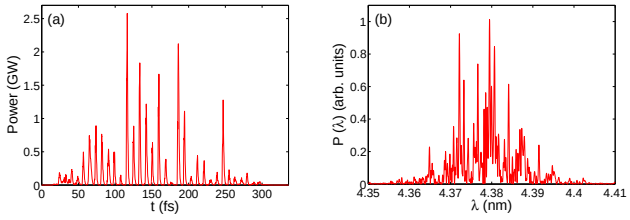

FIG. 9: FEL power and spectrum without a coherent seed.

Because the FEL starts from shot noise, here it requires 8 undulator sections to reach the GW level. For the current-enhanced SASE case, while we still get short pulse trains, the spectrum shows spiky structure instead of equally spaced sharp lines because there is no phase relation between each individual pulse. Furthermore, the power fluctuation of each individual pulse is much larger than the seeded case.

B. Mode-locked multichromatic x-rays for Copper L_3-edge

Both LCLS and LCLS-II can deliver x-rays at the Copper L_3-edge. For LCLS-II, generation of multichromatic x-rays at the Copper L_3-edge can be similarly studied as that in above section for Carbon K-edge. Here we focus on generation of mode-locked multichromatic x-rays at LCLS, which may be tested in the near future.

Currently, a hard x-ray self-seeding experiment is being performed at LCLS. Specifically, one of the 33 undulator sections (U16) has been replaced with a compact chicane which allows installation of a crystal to generate monochromatic radiation following the main SASE pulse generated in U1∼U15 [5]. The electron beam is delayed by the chicane and is further used to amplify the monochromatic radiation in the second half of the undulator sections. At the same time, test of self-seeding in the soft x-ray wavelengths is also being planned. Similarly, one of the undulator section will be replaced with a chicane to accommodate the grating-based monochromator for soft x-ray self-seeding. With the soft x-ray self-seeding configuration completed in the near future, it will be straightforward to test the concept of mode-locked x-rays at LCLS, which only requires installation of a short undulator before the main x-ray undulators.

The beam distribution used for this study is obtained from a start-to-end simulation with 150 pC charge. In the simulation, after the photoinjector the beam slice energy spread was increased to 20 keV with a laser heater to suppress the microbunching instability [39]. After a two-

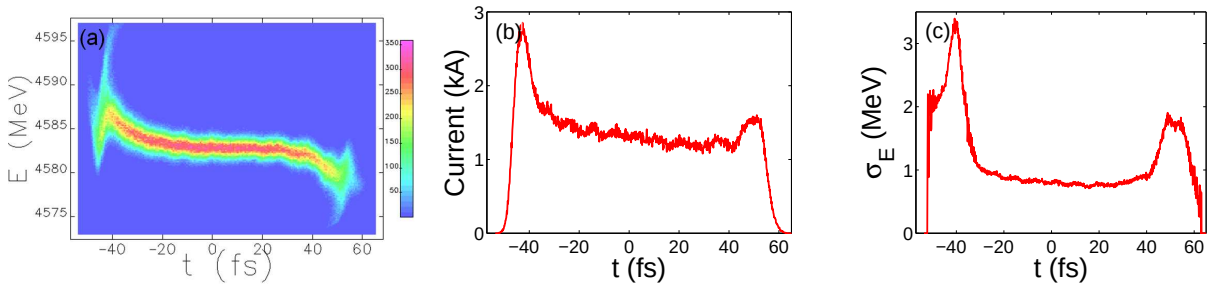

FIG. 10: Electron beam longitudinal phase space (a); Electron beam peak current distribution (b); Electron beam slice energy spread (c).

stage bunch compression with a compression factor of about 35, the beam peak current was increased to about 1.2 kA and the slice energy spread was correspondingly increased to about 800 keV. The beam longitudinal phase space, peak current and slice energy spread are shown in Fig. 10.

We assume the 7th undulator U7 in LCLS is replaced with a small chicane for implementing the self-seeding technique. The energy modulation amplitude and wavelength are taken to be the same as that used in section above, except that the laser rms pulse width is assumed to be 30 fs. With a grating to provide a resolving power of 7500, the spectrum and power of the monochromated radiation is shown in Fig. 11 (here the overall efficiency of the monochromator is assumed to be 1.5%). Note, due to the limited resolving power of the grating, the monochromated radiation actually has multiple modes. Selection of a single mode can be achieved either with a shorter electron bunch, or with a grating having higher resolving power.

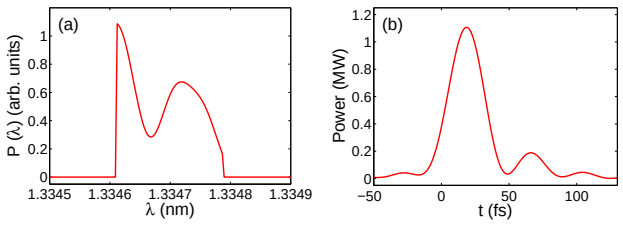

FIG. 11: FEL spectrum (a) and power (b) after the monochromator.

With similar procedures, the coherent seed after amplification in 5 undulator sections is translated to a mode-locked output as shown in Fig. 12. The peak power of the short pulse train exceeds 20 GW and the total number of photons is about 1.4×10^{12}. The FWHM bandwidth of each frequency line is about 1.2×10^{-4}. The FEL power can be further increased with more undulator sections at the cost of degraded spectrum purity.

It should be pointed out that the power of the coherent seed from the monochromator has nearly 100% fluctuation, which will affect the power and spectrum of the final output. Driving the FEL to deep saturation is expected to reduce the power fluctuation, but it will likely result in degradation in spectrum purity. This is because close to the saturation region, the growth of the FEL power starting from the coherent seed slows down, but that from SASE process may still lie in the exponential regime and thus will make more contribution to the total FEL power.

It is worth mentioning that in principle one can use a multi-slit in the grating-based monochromator to select multiple seeds at different frequencies and amplify them in U2 to realize multichromatic x-rays. However, this scheme may have a much larger fluctuation in FEL power and spectrum. If the probability to have a decent power after the monochromator for a single-frequency seed is P ($P < 1$), then the probability to have decent power simultaneously for N seeds is P^N. Furthermore, in our proposed scheme, the FEL output is naturally synchronized with the laser used to generate density modulation in electron beam. Therefore, the proposed scheme may provide higher temporal resolution for time-resolved spectroscopy.

V. SUMMARY AND OUTLOOK

We have studied a simple scheme to generate mode-locked multichromatic x-rays in an FEL. It is found that by using a laser to imprint periodic modulation in electron beam phase space, a single-frequency coherent seed can be amplified and further translated to a mode-locked multichromatic output in an FEL. In the time domain, the mode-locked multichromatic x-rays is characterized by short pulse trains with spacing equal to the laser wavelength. Accordingly, in frequency domain the mode-locked output has a series of equally spaced sharp lines, which may offer the capability to explore the structure and dynamics of a large number of atomic states simultaneously. While we focused on generating mode-locked x-rays in the soft x-ray wavelengths, we believe it is straightforward to apply the technique to generate mode-locked x-rays in the hard x-ray wavelengths as well. As we pointed out earlier, the fluctuation of the coherent seed will likely result in a moderate fluctuation in the

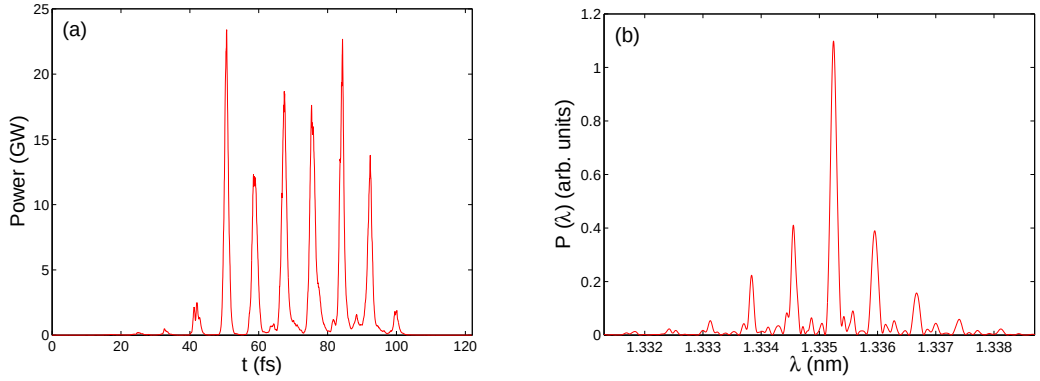

FIG. 12: FEL power and spectrum after the coherent seed is amplified by the density-modulated beam in 5 undulator sections.

final FEL output. We plan to address the statistic performance of the mode-locked FEL in the future.

The mode spacing and number of modes of the FEL output can be varied by changing the modulation laser wavelength and energy modulation amplitude. This allows one to tailor the FEL output for specific applications. Furthermore, the FEL output is naturally synchronized with the modulation laser, which is very desirable for time-resolved spectroscopy and other pump-probe experiments. We anticipate that the mode-locked multichromatic x-rays may open new opportunities in various areas of x-ray sciences.

Finally, it is worth mentioning that several existing schemes [40–44] that use external seeding and a few-cycle infrared laser to generate an isolated attosecond pulse can be extended to generate attosecond pulse train with multiple sharp frequency lines if the few-cycle infrared laser is replaced with an ordinary multiple-cycle laser. For instance, in Ref. [41], an isolated attosecond x-ray pulse with central wavelength at 1 nm and FWHM pulse width of 20 attosecond was generated. If a train of 20 attosecond pulse is generated using multiple-cycle Ti:sapphire laser, then in frequency domain there will be ∼50 sharp lines equally separated by 1.5 eV. With a high repetition rate electron beam and a high repetition rate carrier envelope phase stable laser, one may even achieve tens of thousands frequency lines with equal spacing, i.e. the x-ray frequency comb [45]. The work reported here is one simple example of manipulating x-rays. We believe having the ability to manipulate and control the x-rays will have profound implication for the x-ray science in the future, such as x-ray communications and x-ray frequency comb.

VI. ACKNOWLEDGEMENTS

We thank Y. Feng, J. Guo and V. Strocov for useful discussions. This work was supported by the U.S. DOE under Contract No. DE-AC02-76SF00515.

[1] A. Kondratenko and E. Saldin, Part. Accel. 10, 207 (1980).
[2] R. Bonifacio, C. Pellegrini, and L.M. Narducci, Opt. Commun. 50, 373, (1984).
[3] J. Feldhaus, E.L Saldin, J.R Schneider, E.A Schneidmiller and M.V Yurkov, Opt. Commun. 140, 341 (1997).
[4] Y. Ding, Z. Huang and R. Ruth, Phys. Rev. ST Accel. Beams 13, 060703 (2010).
[5] G. Geloni, V. Kocharyan, and E. Saldin, DESY Report No. 10-033, 2010.
[6] G. Geloni, V. Kocharyan, and E. Saldin, DESY Report No. 10-053, 2010.
[7] L.-H. Yu, Phys. Rev. A 44, 5178 (1991).
[8] L.-H. Yu *et al.*, Science 289, 932 (2000).
[9] G. Lambert *et al.*, Nat. Phys. 4, 296 (2008).
[10] T. Togashi *et al.*, Opt. Express 19, 317 (2011).
[11] G. Stupakov, Phys. Rev. Lett. 102, 074801 (2009).
[12] D. Xiang and G. Stupakov, Phys. Rev. ST Accel. Beams 12, 030702 (2009).
[13] D. Xiang *et al.*, Phys. Rev. Lett. 105, 114801 (2010).
[14] D. Xiang *et al.*, Phys. Rev. Lett. 108, 024802 (2012).
[15] Luuk J.P. Ament *et al.*, Rev. Mod. Phys. 83, 705 (2011).
[16] J. Carlisle *et al.*, Phys. Rev. Lett. 74, 1234 (1995).
[17] Y. Harada *et al.*, Phys. Rev. B 66, 165104 (2002).
[18] L.-C. Duda *et al.*, Phys. Rev. Lett. 96, 067402 (2006).
[19] J. Schlappa *et al.*, Phys. Rev. Lett. 103, 047401 (2009).
[20] L. Braicovich *et al.*, Phys. Rev. Lett. 104, 077002 (2010).
[21] V. Strocov, J. Synchrotron Rad. 17, 103 (2010).
[22] N.R. Thompson and B.W.J. McNeil, Phys. Rev. Lett. 100, 203901 (2008).
[23] D.J. Dunning, N.R. Thompson and B.W.J. McNeil, Proceedings of FEL2010, p636, Malmo, Sweden, 2010.
[24] E. Kur, D.J. Dunning, B.W.J. McNeil, J. Wurtele and A.A. Zholents, New J. Phys, 13, 063012 (2011).

[25] P. Emma *et al.*, Nat. Photon. 4, 641 (2010).
[26] W. Ackermann *et al.*, Nat. Photon. 1, 336 (2007).
[27] D. Pile, Nat. Photon. 5, 456 (2011).
[28] LCLS-II Conceptual Design Report, unpublished, 2011.
[29] M. Xie, Proceedings of PAC95, p183 (1995).
[30] V.N. Strocov *et al.*, J. Synchrotron Rad. 17, 631 (2010).
[31] D. Xiang and G. Stupakov, Proceedings of FEL10, p282, Malmo, Sweden, 2010.
[32] M. Borland, "Elegant: A flexible SDDS-compliant code for accelerator simulation," Advanced Photon Source LS-287, September, (2000).
[33] S. Reiche, Nucl. Instrum. Methods Phys. Res., Sect. A 429, 243 (1999).
[34] Y. Feng *et al.*, *Compact Grating Monochromator Design for LCLS-I Soft X-ray Self-Seeding*, unpublished, 2011.
[35] Y. Feng, private communications.
[36] K. Bane and G. Stupakov, in Proceedings of the 21st Particle Accelerator Conference, Knoxville, 2005 (IEEE, Piscataway, NJ, 2005).
[37] Y. Ding *et al.*, Phys. Rev. ST Accel. Beams 14, 120701 (2011).
[38] A. Zholents, Phys. Rev. ST Accel. Beams, 8, 040701 (2005).
[39] Z. Huang *et al.*, Phys. Rev. ST Accel. Beams 13, 020703 (2010).
[40] A. Zholents and W. Fawley, Phys. Rev. Lett, 92, 224801 (2004).
[41] D. Xiang, Z. Huang and G. Stupakov, Phys. Rev. ST Accel. Beams, 12, 060701 (2009).
[42] A. Zholents and G. Penn, Nucl. Instrum. Methods Phys. Res., Sect. A 612, 254 (2010).
[43] J. Yan *et al.*, Nucl. Instrum. Methods Phys. Res., Sect. A 621, 97 (2010).
[44] J. Qiang and J. Wu, Appl. Phys. Lett, 99, 081101 (2011).
[45] A. Cingöz *et al.*, Nature 482, 68 (2012).